

Silver Nanoparticle Biosynthesis Using Aqueous Leaf Extract of *Ziziphus Spina-Christi* (L): Characterization, Biological and Environmental Applications

Nabil A. Alhemiary^{1,2*}, Ahmed N. Al-Hakimi^{2,3}, Ibrahim A. Alhagri^{2,3} and Sadeq M. Al Hazmy³

¹Department of Chemistry, College of Science and Arts- Sharourah, Najran University, Sharourah, Saudi Arabia

²Department of Chemistry, College of Science, Ibb University, P. O. Box 70270, Ibb, Yemen

³Department of Chemistry, College of Science, Qassim University, Buraidh, Saudi Arabia

*Correspondence: nafarhan@nu.edu.sa Received: August 12, 2024, Revised: Sep., 19 2024, Accepted: Sep., 20, 2024 e-Published: September 10, 2024

The current work focused on the environmentally friendly manufacture of silver nanoparticles using *Ziziphus spina-christi* (L) leaves. The study employed the aqueous leaves extract, which contains alkaloids, coumarins, and flavonoids, as a reducing and stabilizing agent in the easy bio-fabrication of silver nanoparticles (Zs-AgNPs). The crystalline nanoparticle formation of the biologically produced Zs-AgNPs was confirmed and examined using scanning electron microscopy (SEM), zeta potential measurement, energy dispersive X-ray (EDX), and UV spectroscopy. Zs-AgNPs were shown to have a monoclinic structure with a crystallite diameter of 9 nm using XRD analysis. The TEM and SEM morphological images of Zs-AgNPs is confirmed by their spherical shape and smooth surface. The Zs-AgNPs were shown to be stable at pH 10 and to have a high bandgap and substantial optical absorbance in the UV region at 421 nm, which suggests the presence of charge carriers and surface oxygen vacancies. Using FT-IR and EDX spectroscopy, the presence of Ag and O elements as well as their Ag bonds was determined. UV light irradiation was used to study the photodegradation of aqueous 0.1% Eosin Y dye. After 120 minutes of irradiation, a maximum degradation efficiency of 89.5% was achieved. Additionally, Zs-AgNPs were employed as antifungal and antibacterial agents against two fungi and six Gram-positive and Gram-negative bacteria. Additionally, the DPPH assay was used to compare the antioxidant activity of biologically and chemically synthesized AgNPs. The results showed that the biosynthesized nanoparticles had significantly higher antioxidant activity than the chemically synthesized nanoparticles, and this finding could have significant applications in the biomedical field. Biosynthesis of Zs-AgNPs is environmentally friendly and inexpensive, as well as yields highly stabilized nanoparticles by phytochemicals.

Keywords: *Ziziphus spina-christi* (L), Photodegradation, Biosynthesis, silver nanoparticles, Eosin Y dye.

INTRODUCTION

Ziziphus spina-christi (L), a tree that may grow to a height of 20 meters, is locally known as Sidr and is also generally known as Christ's thorn or Jerusalem thorn in English (El Maaiden et al., 2019). This kind of tree is multifunctional and belongs to the Rhamnaceae family of plants. One of the few really native tree species in Arabia (Saudi Arabia, Jordan, Yemen, and Egypt), it is an important cultivated tree that continues to flourish alongside several recently imported exotic plants (Ads et al., 2018). The leaves of *Z. spina-christi* are also used as an anti-inflammatory in folk medicine for wounds, eye conditions, bronchitis, and skin ailments (Dkhil et al., 2018). Furthermore, it has a strong effect in inhibiting and even killing bacteria (Al-Maaqar et al., 2022, El Maaiden et al., 2019). According to reports, it is

effective against fungi and bacteria that are often very resistant to contemporary treatments (Alotibi et al., 2020). As such, it is used to treat fever, diarrhea, and respiratory conditions including TB, cough, and bronchitis. It also helps to speed up the healing of recently opened wounds. Four different forms of glycosides known as christinin-A, B, C, and D are found in the purified butanol extract of *Z. spina-christi* leaves (Amin et al., 2020). Secondary metabolites found in leaves include tannins, alkaloids, flavonoids, polyphenols, and saponins (Amin et al., 2020). Green NP synthesis has consistently drawn a lot of interest due to its advantages over chemical and physical approaches, including its low cost, environmental friendliness, and lack of need for hazardous chemicals, high pressure, energy, or

temperature (Hembram et al., 2018). The green chemistry criteria are utilized in biological approaches to substitute harsh chemicals with natural products such as biodegradable polymerase, enzymes, and phytochemicals. Metal salts are rapidly reduced, stabilized, and capped by biomolecules found in plant components such as alkaloids, flavonoids, and other phenolic compounds (lignin, phenolic acids, tannins, and stilbenes)(Chapagain et al., 2022).

Among the various noble metals, silver (Ag) exhibits remarkable antimicrobial, antiviral, and biocompatible properties, showing promising potential for biomedical applications and those involving microbial resistance, sunscreen lotions, molecular imaging contrast agent, DNA detection, wound healing, drug delivery, diagnostic and treatment of diseases, and food packaging(Abdelsattar et al., 2022). Researchers are more interested in silver nanoparticles (AgNPs) than in nanoparticles composed of noble metals because of their distinct physical and chemical characteristics, which include excellent electrical conductivity, strong chemical stability, thermal and nonlinear optical properties(Zhang et al., 2016). AgNPs size, composition, and form can all significantly affect how effective they are. Researchers have been interested in silver nanoparticles (AgNPs) due to their potent biological properties, which include antioxidant, wound-healing, antibacterial, and anticancer activities(Zhang et al., 2016).

Many studies have reported the synthesis of silver nanoparticles using extracts from different plant morphological sections, such as flowers, leaves, stems, or seeds(Hembram et al., 2018). Because of this, the phytochemical composition of each plant varies, yet their shared characteristics define their distinct characteristics(Zheljazkov et al., 2018). AgNPs size, shape, and stability are essentially determined by physicochemical and technical factors, including the reaction mixture's temperature, pH, and reaction ratio, as well as the extract's preparation technique and solvent type(Balciunaitiene et al., 2021). There have been reports of silver nanoparticle production from several plant extracts, including *Eugenia roxburghii* DC (Giri et al., 2022), *Clerodendrum inerme* (Manikandan et al., 2021), *Aloe vera*(Anju et al., 2021), *Euphorbia sanguine* (Ekennia et al., 2022), *Acacia nilotica* (Alduraim et al., 2023), *Premna integrifolia* L.(Singh et al., 2023), *Saccharum officinarum*, (Noppradit et al., 2023), *Sambucus ebulus*(Karan et al., 2024), and *Spirulina platensis* (Gul et al., 2024). Nevertheless, there is a lack of knowledge regarding the biological uses of silver nanoparticles derived from *Z. spina-christi* (L) or their manufacture.

Therefore, the aim of this study was to synthesize AgNPs using green synthesis technology, using *Z. spina-christi* (L) leaf extract collected during March and April 2024 from Najran region, Saudi Arabia, as a reducing agent. The synthesized AgNPs were then

characterized, and their antifungal, antioxidant and antibacterial activity was investigated.

MATERIALS AND METHODS

Materials

The leaves fresh and young of the locally grown *Z. spina-christi* plant leaves were collected from in Sharourah, Najran- Saudi Arabia. The chemicals and media used in This study were all purchased from Sigma-Aldrich in Darmstadt, Germany.

Z. spina-christi Extract Preparation

The leaves were carefully cleaned with double-distilled water and allowed to air dry at room temperature for a period of three weeks. A powder was created by grinding the dried leaves. Afterwards, reflux condensation was performed for 30 minutes at 60°C for a mixture of 10 g of powder with 100 ml of double distilled water. After that, the extract was let to cool to ambient temperature. Whatman No. 1 filter paper was used to filter the extract that had become yellow.

Synthesis of Zs-AgNPs

Z. spina-christi extract was added to AgNO₃ aqueous solution 1 mM in 1:10 dilution at ambient temperature and stirred continuously for 30 minutes at 400 rpm to create Zs-AgNPs. The solution's color changed from yellow to dark brown, indicating the creation of AgNPs (Yu et al., 2019). The 0.1 M NaOH was used to keep the pH of the solution at 10. It was noted that the solution's color changed. To verify that AgNPs were formed, the UV-vis spectra were taken at various intervals. A Sigma centrifuge was used to centrifuge the totally reduced solution for 20 minutes at 25 °C at 10,000 rpm. After discarding the supernatant liquid, the particle was again dispersed in distilled water. To remove any material that had adhered to the surface of the silver nanoparticles, the centrifugation procedure was carried out three times, and the last step involved the use of pure ethanol. To prepare them for additional examination, the purified AgNPs were dried at room temperature and placed in an aluminum foil-covered Eppendorf tube.

Zs-AgNPs Characterization Method and Instrument

Many methods were used to examine the thermal stability, surface, structural morphology, and optical characteristics of the bio-fabricated Zs-AgNPs. UV-Vis spectroscopy (6850 UV-Vis spectrophotometer, Jenway, USA) was used to measure the absorbance of the Zs-AgNPs in the 300–700 nm wavelength range. The Zs-AgNPs surface chemistry and the role of phytochemical functional groups in the bio reduction and capping process were investigated using Fourier Transform Infrared spectroscopy (FT-IR) and a Shimadzu Irtfinity-1. The 4000–400 cm⁻¹ range was used for the FT-IR investigation. The value of the zeta potential aids in the

comprehension of the forces interacting between particles. Using Zetasizer Nano Series ZS, the hydrodynamic size of Zs-AgNPs and Zeta potential were determined in the AgNPs solution. Using energy-dispersive X-ray (EDX) analysis, Zs-AgNPs were elementally constructed. TEM was employed, nonetheless, to determine Zs-AgNPs' dimensions and shape. The bio-fabricated Zs-AgNPs were washed with deionized water many times in preparation for TEM analysis. The samples were put on a copper grid that had been covered with carbon, removed, and allowed to cure before being examined. A Transmission Electron Microscope (JEOL, JEM1011, Tokyo, Japan) was used for TEM analysis to determine the size, morphology, and particle size distribution. At 100 kv voltage, this microscope provided high-resolution two-dimensional images. The crystalline characteristics of the produced nanomaterials were assessed by XRD analysis, and the hydrodynamic particle size and net charge of the Ag nanoparticles were ascertained by zeta potential measurement (Tang et al., 2020). To perform the X-ray powder diffraction (XRD) investigation, a Shimadzu LabX XRD-6100 diffractometer was equipped by a graphite monochromator that generated Cu-K radiation.

Biogenic Zs-AgNPs' Photocatalytic Dye Degradation Activity

The disintegration of Eosin Y dye was observed by the photocatalytic activity of biogenic AgNPs when exposed to UV radiation. Every dye was prepared in an aqueous 0.1% solution. Dyes were first combined with a 10 mg/mL concentration of Zs-AgNP. The solution was subjected to UV light for the following durations: 0, 5, 10, 15, 30, 60, 90, and 120 minutes. To determine the percentage of dye degradation, the following formula was used (Wijesinghe et al., 2021).

$$\text{Degradation efficiency (\%)} = \frac{C_o - C}{C_o} \times 100$$

Where C represents the maximum peak absorbance at a specific time and C₀ represents the greatest peak absorbance at 0 min.

Antibacterial Activity Estimation

The resulting Ag-NPs were evaluated for their ability to inhibit six different strains of Gram (-) and Gram (+) bacteria. This included *E. coli*, *P. aeruginosa*, *S. pneumonia*, *K. pneumonia*, *S. epidermis*, and *S. aureus*. The Disc diffusion technique was used to examine the solutions containing Ag-NPs particles and the plant leaf extract. The discs were air dried in a sterile environment after being individually soaked in 100 ul of double distilled water, silver nitr nitrate (+control), and Ag-NPs solution. The bacteria cultures were swabbed with the nutritional agar media aureus plates. AgNP/disc was present in a concentration of 25 mg/mL. After incubating

the samples for 16 hours at 37 °C, the inhibition zones were visible, and the sample with the largest zone of inhibition was recorded.

Antioxidant Activity of Zs-AgNPs

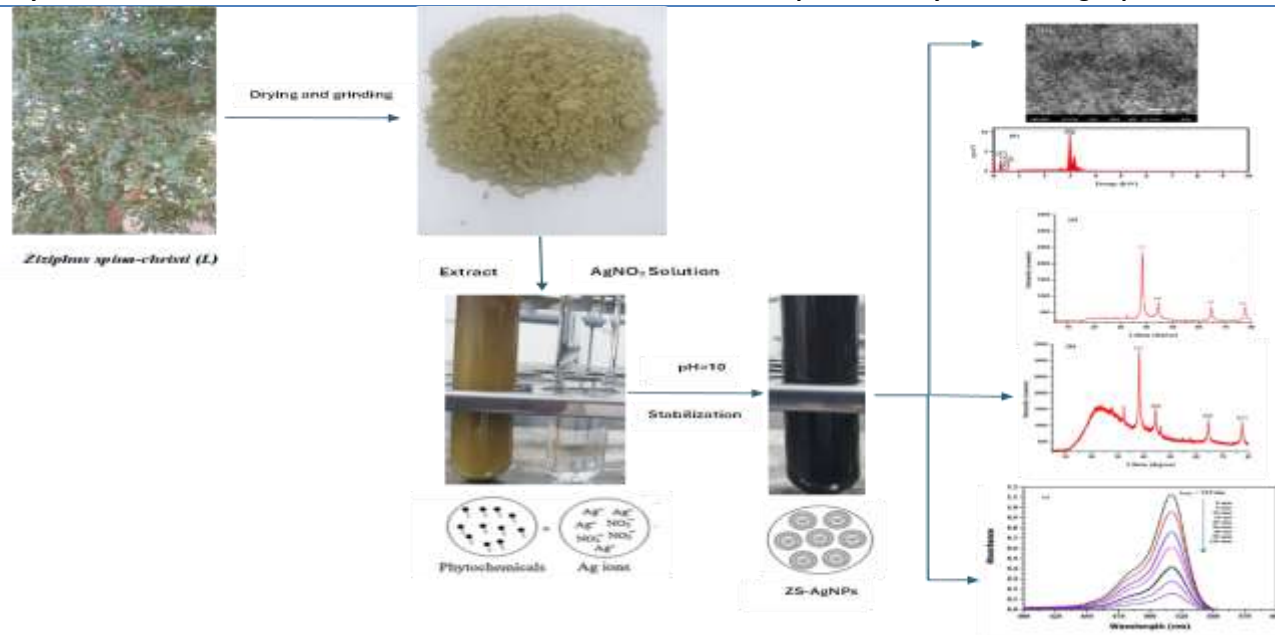
The antioxidant capacity of Zs-AgNPs was assessed using the DPPH (2,2-diphenyl-1-picrylhydrazyl) free radical scavenging test. MilliQ water was used to create 5 ml of ascorbic acid in various doses (2 µg/ml, 4 µg/ml, 6 µg/ml, 8 µg/ml, and 10 µg/ml). A test tube was filled with one milliliter of the silver colloidal solution and one ml of ascorbic acid in each concentration. Following that, 450 µL of Tris-HCl buffer (50 mM/pH 7.6) and 1 mL of 0.01 mM DPPH (dissolved in methanol) were added, and the mixture was shaker-conditioned (100 rpm) at 37 °C for 40 minutes in the dark (Fouda et al., 2022) (ERENLER et al., 2021). gNPs or ascorbic acid were swapped out for one milliliter of Milli-Q, which was used as a blank to conduct an additional series of tests. The color's produced absorbance was measured at 517 nm (Sreelekha et al., 2021). The following formula was used to determine the percentage of radical-scavenging activity:

$$\% \text{ DPPH Radical Scavenging Activity} = \frac{AC - AS}{AC} \times 100 \quad (2)$$

AC is absorbance control, AS is absorbance sample.

The biogenic Zs-AgNPS Antifungal Activity

Nanomaterial seeding medium were used to assess the antifungal activity of the silver nanoparticles against *F. chlamydosporum* and *A. flavus*. After autoclaving, the PDA medium was chilled to around 45 °C. After that, the medium was supplemented with silver nanoparticles at final concentrations of 0, 50, 100, 150, and 200 ppm. Mycelial plugs with a diameter of about 3 mm were removed from the edge of cultures of the tested fungi that were 7 days old. They were then aseptically seeded upside down onto the PDA that contained nanoparticles. At 27 ± 2 °C, the plates were incubated (three copies for each treatment). The examined fungi's growth was monitored for seven days, and the percentage of mycelial growth suppression was contrasted with that of the control (0 ppm silver). Additionally, the dosage necessary for a desired effect in 95% of the fungal culture (ED95) and the median effective dose (ED50) were ascertained.



Scheme 1: Synthetic strategy to prepare Zs-AgNPs

RESULTS AND DISCUSSION

Examining Zs-AgNPs' Optical Characteristics Using UV-Vis Spectroscopy

Zs-AgNPs were synthesized at room temperature when plant extract was added to a 1 mM silver nitrate solution, causing the solution's color to shift from yellow to reddish-brown. The surface plasmon resonance (SPR) action may be the cause of the color creation, and aqueous extracts convert Ag^+ ions to Ag^0 (Adhikari et al., 2022). Using a magnetic stirrer, the plant extract was added drop by drop, revealing the solution's original yellow hue. After 30 more minutes of stirring the reaction mixture (pH 10), the solution took on a dark hue, as seen in Scheme 1. Finally, the solution was allowed to sit at room temperature for 24 hours in the dark to convert Ag^+ to Ag^0 . Even after 24 hours, the mixture's color did not change, and no SPR band was seen at normal circumstances (pH 6.4). Thus, by adding 0.1 M NaOH, the pH of the solution combination was kept constant. Figure 1a shows that an absorption peak that was narrow and sharp was only seen at pH 10, and it was not acquired at other pH levels. Figure 1b displays the UV-vis spectra at different periods. The production of Zs-AgNPs was revealed by the distinctive UV absorption peak at 421nm. As the amount of silver ions in the aqueous solution decreases over time, more Zs-AgNPs may develop, which would explain the spectrum's gradual increase in intensity. A single SPR band was seen in the UV-vis spectra of the produced nanoparticles, confirming the presence of spherically shaped nanoparticles in the solution (Miranda et al.,

2022). The Zs-AgNPs were shown to be stable in the pH 10 solution even one month after they were synthesized. By stability, we mean that the optical characteristics of the nanoparticle solutions did not change noticeably over time.

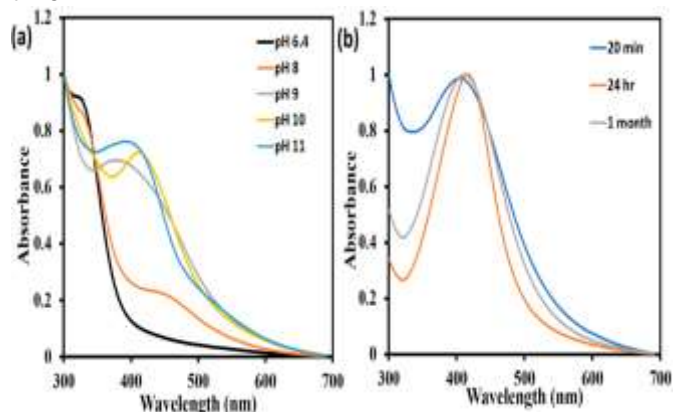


Figure 1: shows the Zs-AgNPs (a) UV-vis spectra at different pH levels and (b) the UV-vis absorbed spectrum at different times.

Analysis Using Fourier-Transformed Infrared (FT-IR)

FT-IR analysis of the *Z. spina-christi* (L) extract revealed several active chemicals that helped with the environmentally friendly creation of nanoparticles (Figure 2). The presence of active molecules responsible for capping and decreasing the particles is indicated by a high peak for OH stretching owing to phenols, N-H and C-H bending for amide and aromatic groups, and C=C stretch for carboxylic or amide groups (Table 1). Lipids, proteins, carbohydrates, and pigments are all present according to the spectrum data (Kendel & Zimmermann, 2020).

Table 1: FT-IR spectra demonstrating the likely functional groups of the Zs-AgNPs and aqueous *Z. spina-christi* (L) extracts.

Wave Number (cm ⁻¹)		Probable Functional Group
<i>Z. spina-christi</i> (L) Extract	Zs-AgNPs	
Lipids (3000-2800 cm ⁻¹)		
	3754	O-H stretch (Alcohols)
3368	3403	N-H stretch (Amine)
Proteins (1700-1500 cm ⁻¹)		
1708	1706	C=C stretch (Benzene), C=O (saturated Aldehyde)
1613	1519	N-H (Amides, Nitro compounds), C=O stretch (Ketone, Carboxylic acids), C-C stretch (Amides), C=C (Benzene, Alkenes)
1530	1526	N-H (Nitro compounds, C=C (Benzene), C-O stretch (Ketone, Amides)
Carbohydrates (1500-1000 cm ⁻¹)		
1448	1445	O-H (Alcohols), CO-H bend (Aldehydes), N=O stretch (Nitro compounds),
1347	1347	C-N stretch (Amines), C-O stretch (Alcohols, Ethers), O-H bend (Carboxylic acids)
1201	1200	C-O stretch (Ethers, Alcohols), O-H bend (Carboxylic acids), C-N stretch (Amines)
1123	1123	C-N stretch (Amines), C-O stretch (Ether, Esters, Alcohol), S=O stretch (Sulfoxides),
1032	1030	N-H (Nitro compounds, Amides), C-C stretch (Amides), C=C (Benzene, Alkenes), C=O stretch (Ketone, carboxylic acids)
Cell wall components and chlorophyll (1000 – 600 cm ⁻¹)		
865	866	C-H bend (Alkenes),
757	756	C-C stretch (Chlorides), C-N stretch (Amins), =C-H bend (Benzene)
665		C-N stretch (Amines), =C-H bend (Benzene), C-C stretch (Chlorides).

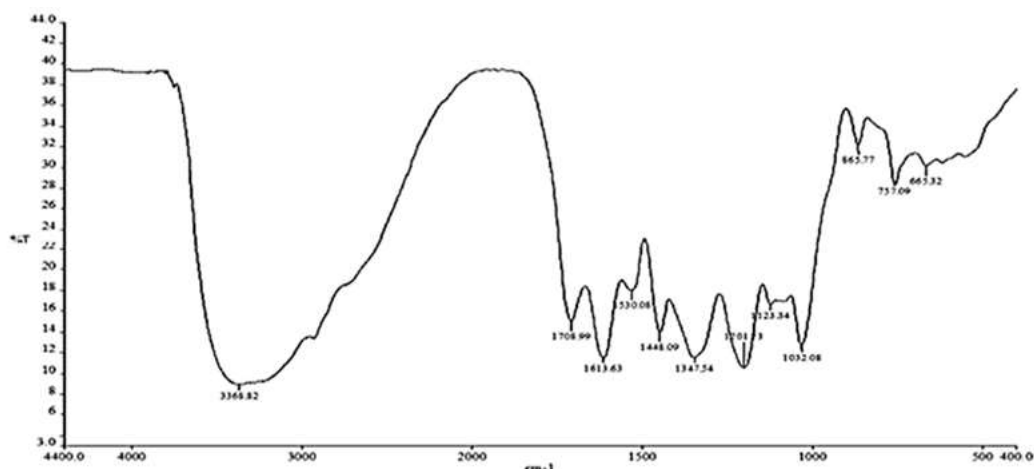


Figure 2: FT-IR analysis of biosynthesized Ag-NPs produced from *Z. spina-christi* (L) aqueous extract.

XRD and TEM Analysis

XRD analysis was utilized to determine the crystalline state of the dried Zs-AgNPs. The XRD pattern of Zs-AgNPs is shown in Figure 3b. There were four distinct diffraction peaks at 38.2, 45.4, 64.1, and 76.9 , respectively corresponding to (111), (203), (220), and (311) planes of face-centered cubic crystal structure of metallic silver (JCPDS file no.040783).

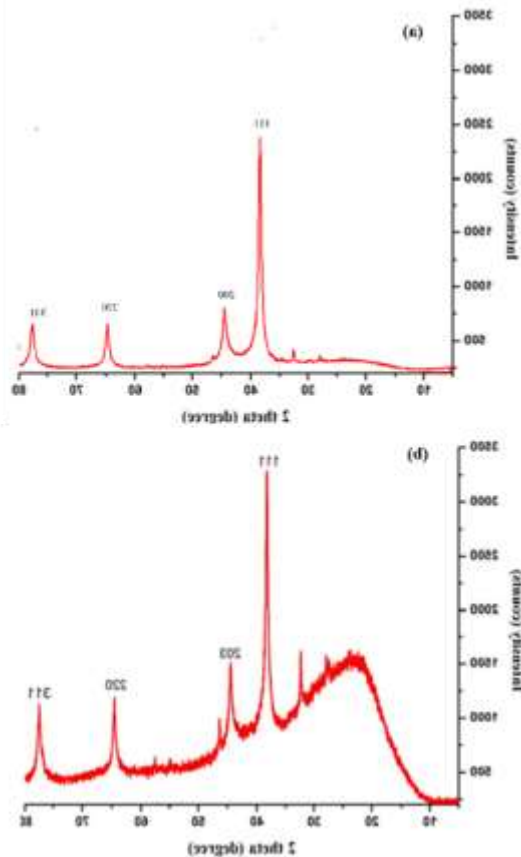


Figure 3: (a) AgNPs XRD pattern, (b) Zs-AgNPs XRD X-ray diffraction pattern of the synthesized material made with *Z. spina-christi* (L) aqueous leaf extract.

Debye-Scherrer equation $D = K\lambda / \beta \cos\theta$ may be used to calculate the crystalline size of the nanoparticles. Here, D stands for crystalline size, K for Scherrer constant (0.98), λ for wavelength (1.54), and β for full width at half maximum (FWHM). 20 nm was determined to be average particle size. The brilliant circular ring pattern seen in SAED, and the diffraction peaks obtained during XRD indicated that the Zs-AgNPs were crystalline in nature. Erigeron bonariensis showed comparable SAED and XRD patterns(Kumar et al., 2016). The produced nanoparticles were spherical in form and had a smooth surface, as demonstrated by the TEM images of the Zs-AgNPs (Figure 4(a)). SAED pattern analysis (Figure 4(b)) further verified the

Silver Nanoparticle Biosynthesis Using Aqueous Leaf Extract

crystalline nature of silver nanoparticles. The average particle size of the Zs-AgNPs was 9 nm, and their particle size distribution ranged from 5 to 15 nm (Figure 4(c)).

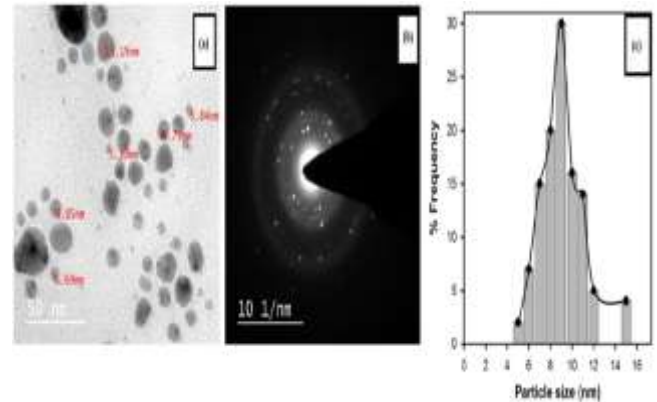


Figure 4: (a) TEM images of Zs-AgNPs at different magnifications, (b) SAED pattern of Zs-AgNPs , and (c) size distribution histogram.

EDX and SEM Analysis Zs-AgNPs

The SEM analysis data showed that the synthesized Zs-AgNPs were spherical in shape of various sizes ranging between 9 and 35 nm (Figure 5(a)). Some nanoparticles were bigger in size, which may be due to aggregation or overlapping of particles. The shape, size, and morphology of synthesized green nanoparticles were confirmed by TEM and SEM imaging. For the purpose of characterizing nanoparticles, these methods have been regularly employed by many researchers(Maduraimuthu et al., 2023). The spherical form and smooth surface of the Zs-AgNPs were confirmed by TEM and SEM pictures, indicating that they were substantially stabilized. In these aggregates, the particles were not directly attached to each other. This suggests that the nanoparticles were stabilized by the aqueous extract of *Z. spina-christi* (L), are surrounded by a thin layer of some capping organic substances from the plant leaf, as seen in the TEM micrograph(EI-Ansary et al., 2018). EDX spectra of silver nanoparticles were observed between 2.5-4 keV, which clearly showed a strong spectral signal in the silver region at 3.3 keV (Figure 6b). The EDX spectrum indicates the existence of biomolecules next to Zs-AgNPs due to the presence of signals for carbon, nitrogen, and oxygen(Sidhu et al., 2022).

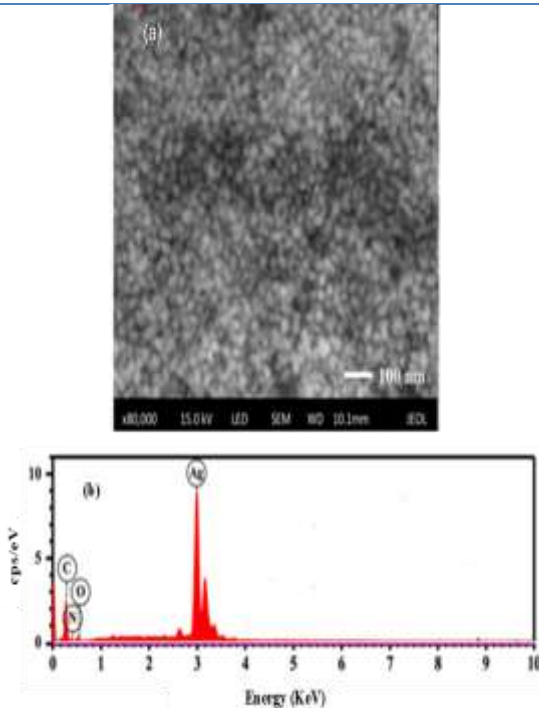


Figure 5: (a) SEM micrograph of AgNPs synthesized using *Z. spina-christi* (L) aqueous leaf extract, (b) energy DXR of Zs-AgNPs.

Assay for Antimicrobials

Green generated Ag-NPs have been evaluated for antibacterial activity against a variety of bacterial species using the zone of inhibition technique. The obtained silver nanoparticles demonstrated positive results in antimicrobial testing. The antibacterial efficacy of silver nanoparticles against a variety of bacterial species was demonstrated by their significant zone of inhibition. Table 2 displays the zone of inhibition for the disc diffusion experiment. The zone of inhibition ranged 9 to 11 mm in diameter for Gram-negative bacteria and 11 to 14 mm in diameter for Gram-positive bacteria. The information gathered is consistent with earlier

research(Ashraf et al., 2019). These Ag-NPs' antibacterial activity may be explained by oxidative stress production, interruption of DNA replication, or direct bacterial cell lysis via AgNP damage to cell membranes (Alsubki et al., 2021). However, the presence of several phenolic chemicals in a single plant extract may be the cause of the antibacterial action. It's also possible that the antibacterial qualities of silver nanoparticles originate from their interactions with hypothetical peptides required for cell proliferation and survival.

Antifungal Activity of Zs-AgNPs

Table 3's data show that the silver nanoparticles inhibited the linear growth of *A. flavus* and *F. chlamydosporum* above than 50% at 200 ppm (ED50 = 159.18, ED95 = 1941.6, slope = 1.75 ± 6.1) and by approximately 50% at 150 ppm (ED50 = 175.78, ED95 = 840.31, slope = 2.31 ± 0.21). The silver nanoparticles' inhibitory impact against *A. flavus* was greater at higher doses than it was against *F. chlamydosporum*. The AgNPs' size, structure, and capping proteins may be responsible for their antifungal action. These results are consistent with the findings of (Yassin et al., 2017) The silver nanoparticles' inhibitory impact against *A. flavus* was greater at higher doses than it was against *F. chlamydosporum*. The AgNPs' size, structure, and capping proteins may be responsible for their antifungal action. These results are consistent with the findings of (Luan & Xo, 2018). The high concentration at which silver nanoparticles may saturate and bind to hyphae in the fluid may be the cause of their strong antifungal action. When the fungus were exposed to silver nanoparticles, their DNA lost its capacity to replicate, which may have caused ribosomal subunit protein expression to be disrupted (Yassin et al., 2021). Overall, especially at high doses, our biogenic silver nanoparticles demonstrated encouraging antifungal activity and could be useful against other test species.

Table 2: Shows the disc diffusion assay-tested antibacterial activity of Zs-AgNPs aqueous leaf extract against bacteria.

Bacterial Strains	Gram stain type	Zone of Inhibition (mm)	
		Control	SZ-AgNPs
<i>E. coli</i>	Gram-negative	8	11
<i>P. aeruginosa</i>		7.5	9
<i>K. pneumonia</i>		8	10
<i>S. pneumonia</i>	Gram-positive	11	12
<i>S. epidermis</i>		10	13
<i>S. aureus.</i>		11	14

Table 3: Biogenic silver nanoparticles' antifungal affect

Nanomaterial concentrations (ppm)	F. chlamyosporum		A. flavus	
	RG	% inhibition	RG	% inhibition
0	91.20	00.00	81.85	00.00
50	81.75	11.28	67.50	17.65
100	64.75	30.17	57.50	31.03
150	53.25	42.94	45.75	45.58
200	40.10	57.67	34.00	60.13
ED ₅₀	175.78		159.18	
ED ₉₅	840.31		1941.6	
Slope ± SE	2.31 ± 0.21		1.75 ± 6.1	

ED₅₀: Entire dosage needed to eradicate 50% of the fungus; In 95% of the fungal culture, ED 95 indicates the dose necessary to get the desired result; "R.G." for radial growth; "Inh. (%)" stands for percentage inhibition.

Antioxidant Activity of Zs-AgNPs

Numerous conditions are linked to oxidative stress, such as atherosclerosis, diabetes, high blood pressure, and cancer. It is interesting to note that tiny quantities of antioxidants (organic chemical substances) can either stop or delay the oxidation of substrates (Jomova et al., 2024). It has been found that metal nanoparticles are an effective antioxidant that counteracts the widespread nitrogen-centered free radical known as DPPH (Naseem et al., 2024). DPPH is a purple-colored, stable free radical with a significant absorption maximum at 517 nm. When an antioxidant is present, the free radicals in the DPPH being coupled off, which reduces absorbance and color intensity. AgNPs giving the DPPH radicals an electron or proton, which is then reduced (Sivalingam et al., 2024). Figure 6 shows the DPPH scavenging activity of chemically and biologically synthesized nanoparticles. For both chemically and biologically synthesized nanoparticles, the percentage of DPPH scavenging activity rose linearly as the nanoparticle concentration increased from 1 to 5 µg/ml. When tested at a concentration of 5 µg/ml, biosynthesized nanoparticles shown 90% of scavenging activity, compared to only 78% for chemically produced ones. Because the surface of the Z. spina-Christi leaf extract nanoparticles contained a bioactive capping agent, they exhibited higher levels of antioxidant activity than the chemically manufactured counterpart. The strong antioxidant activity of flavonoid (Sysak et al., 2023) and phenolic compounds (Sysak et al., 2023) makes them useful for treating and preventing degenerative illnesses. Therefore, the improved antiradical activity near the control ascorbic acid is mostly caused by the bioactive chemicals that are present on the surface of of biosynthesized nanoparticles.

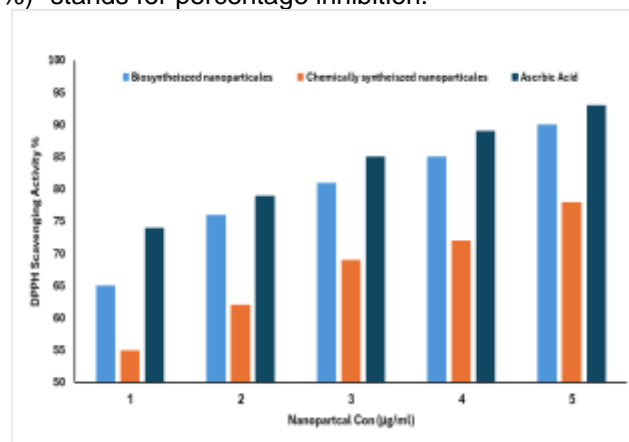


Figure 6: Antioxidant activity of biologically and chemically synthesized AgNPs

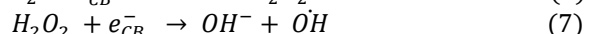
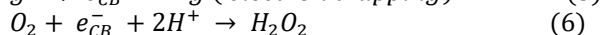
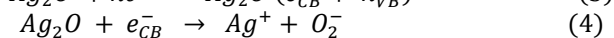
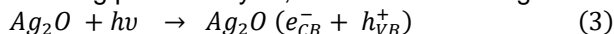
The Photocatalytic Dye Activity Of Zs-Agnps

At various time intervals (0, 5, 10, 15, 20, 30, 60, 90, and 120 min), the photocatalytic dye degradation of aqueous 0.1% Eosin Y dye by Zs-AgNPs under UV light was investigated, as indicated in Figure 7(a). Zs-AgNPs were employed as a catalyst to monitor the dye degradation process using UV-vis spectroscopy. The wavelength range in which the absorption spectra were measured was 400–600 nm. In the visible region, the maximum absorption peak of eosin dye was observed at 515 nm as shown in Figure. 7(a). It was observed that the intensity of the absorption spectrum decreases with respect to time. It's possible that Zs-AgNP-induced redox reactions are to blame for this. According to Figure 7(b), after 120 minutes, the dye had deteriorated by 89.5%. The photocatalyst material absorbs photons and generates an electron-hole pair, which then performs oxidation and reduction reactions on the surface to form super hydroxyl molecules. During the dye degradation process, these molecules chemically react with the dye molecules on the surface of the nanoparticles, increasing surface area availability and thus improving photocatalytic efficiency. Zs-AgNPs thus serve as a source for the electron transfer process. The photocatalytic activities of Zs-AgNPs under UV light may

be facilitated by their Surface Plasmon Resonance characteristic (Aisida et al., 2019). Pathological laboratories routinely utilize eosin dye for regular examinations and the identification of illnesses mediated by bacteria or fungus. However, managing or removing such dye correctly is time-consuming and detrimental to the environment. Therefore, the Zs-AgNP mediated dye degradation technique is still advantageous when it comes to managing pathological waste (Ghatage et al., 2023).

The Mechanism

The high stability of Zs-AgNPs is one of its interesting attributes, resulting in high photocatalytic activity. The partial production of metallic Ag on the Ag₂O surface caused by photocatalysis of organic materials contributes to the stability of the nanophotocatalysts. The photocatalysis process is enhanced by the metallic Ag's participation in the organic pollutants' photodegradation (Loka & Lee, 2022). The equations (3)(10) describe the photocatalysis mechanism and the self-stabilization process of Ag₂O-NPs during photocatalysis, which is seen in Figure 8.



The Zs-AgNPs photocatalyst absorbs photons upon irradiation, leading to the creation of an electron-hole pair (Equation (3)), whereby the hole (h⁺) travels to the valence band (VB) and the electron (e⁻) goes to the conduction band (CB). The Ag⁺ lattice collects the photogenerated electrons (Equation (4)) into the CB of the ZS-AgNP because Ag₂O has a higher negative potential (0.2 V vs. NHE) than Ag⁺/Ag (0.7991 V vs. NHE) but a more positive potential when compared to O₂/H₂O (-0.046 V vs. SHE). On the surface of Ag₂O, metallic Ag is formed because of Ag⁺ reduction. During the multistep photocatalysis, these metallic Ag clusters that have formed on the photocatalyst surface function as an electron pool (Loka & Lee, 2022). Equations (5) and (6) predict that when a given quantity of metallic Ag has accumulated, the subsequent photogenerated electrons will transport in a multielectron way to the metallic Ag sites. Equations (7) to (10) show that when the generated hydrogen peroxide takes an electron and the surface water molecule absorbs the holes in the valence band, a reactive hydroxyl radical species is formed that assaults the organic material and gets rid of the organic contaminant, such organic dyes. Moreover, the target organic pollutant is directly oxidized in accordance with equation (10) (Zidane et al., 2022) as a result of the direct capture of the organic molecule's photoinduced holes, as shown in Figure 8.

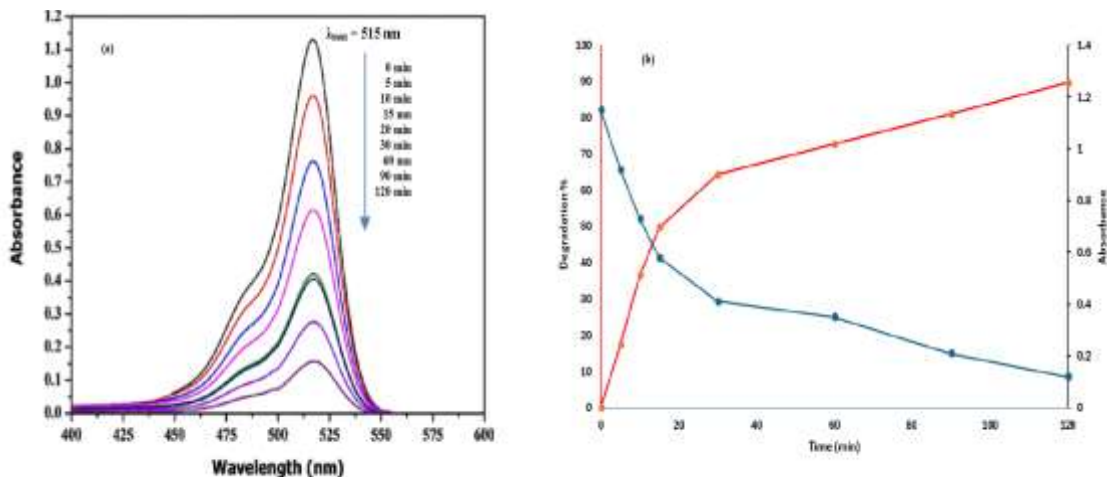


Figure 7: (a) Reaction time's effect on Zs-Ag₂ONPs' Eosin Y degradation; (b) absorption and degradation as a function of time.

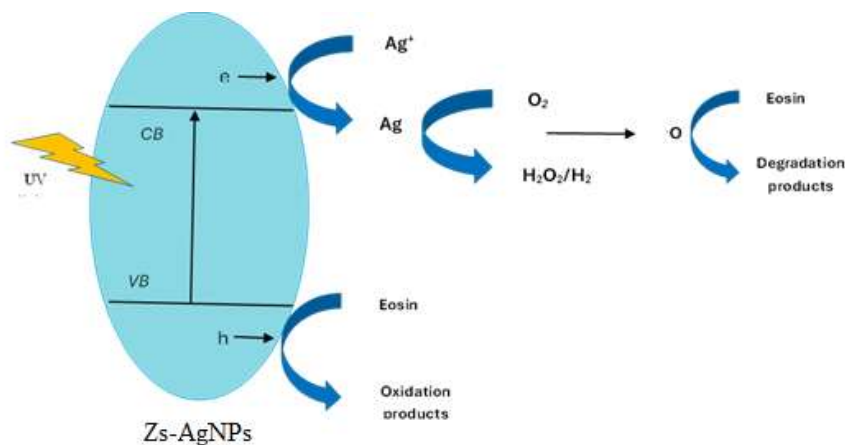


Figure 8: The schematic representation of a potential process for Zs-AgNPs leaf extract-mediated photocatalytic degradation of Eosin Y dye.

CONCLUSIONS

In this study, an aqueous extract of *Z. spina-christi* (L) leaves was used to produce Zs-AgNPs based on phytochemicals. Numerous spectroscopic and microscopic methods were employed to assess the structural characteristics of the biofabricated Zs-AgNPs. The mean particle size of the bio-fabricated Zs-AgNPs was 9 nm. The bio-fabricated Zs-AgNPs effectively acted as a photocatalytic agent to degrade 0.1% Eosin Y dye when exposed to UV light. Additionally, ZS-AgNPs were employed as antifungal and antibacterial agents against two fungi and six Gram positive and Gram negative bacteria. Based on the results, Zs-AgNPs might be a good choice for photocatalytic removal of poisonous dye, pathogenic deactivators, and wastewater treatment.

Supplementary materials

The supplementary material / supporting for this article can be found online and downloaded at: <https://www.isisn.org/article/>

Author contributions

Conceptualization, Nabil A. Alhemiary and Ahmed N. Al-Hakimi; methodology, Nabil A. Alhemiary and Ahmed N. Al-Hakimi.; validation, Ibrahim A. Alhagri and Sadeq M. Al Hazmy.; formal analysis, Nabil A. Alhemiary.; investigation, Ahmed N. Al-Hakimi.; resources, Sadeq M. Al Hazmy.; data curation, Nabil A. Alhemiary and Ibrahim A. Alhagri; writing-original draft preparation, Nabil A. Alhemiary.; writing-review and editing, Ahmed N. Al-Hakimi and Sadeq M. Al Hazmy.; visualization, Y.P.; supervision, J.Q. and P.X.; project administration, Nabil A. Alhemiary. All authors have read and agreed to the published version of the manuscript.

Funding statement

There are no funding sources.

Institutional Review Board Statement

Not applicable

Informed Consent Statement

Not applicable.

Data Availability Statement

All of the data is included in the article/Supplementary Material.

Acknowledgments

We thank ABCD for editing the English text of a draft of this manuscript. We thank our colleagues in our laboratories for their help.

Conflict of interest

The authors declared that present study was performed in absence of any conflict of interest.

Copyrights: © 2024@ author (s).

This is an **open access** article distributed under the terms of the **Creative Commons Attribution License (CC BY 4.0)**, which permits unrestricted use, distribution, and reproduction in any medium, provided the original author(s) and source are credited and that the original publication in this journal is cited, in accordance with accepted academic practice. No use, distribution or reproduction is permitted which does not comply with these terms.

Publisher's note/ Disclaimer

All claims stated in this article are solely those of the authors and do not necessarily represent those of their affiliated organizations, or those of the publisher, the editors and the

reviewers. Any product that may be evaluated in this article, or claim that may be made by its manufacturer, is not guaranteed or endorsed by the publisher. ISI/Net remains neutral with regard to jurisdictional claims in published maps and institutional affiliations. ISI/Net and/or the editor(s) disclaim responsibility for any injury to people or property resulting from any ideas, methods, instructions or products referred to in the content.

Peer Review: ISI/Net follows double blind peer review policy and thanks the anonymous reviewer(s) for their contribution to the peer review of this article.

REFERENCES

- Abdelsattar, A. S., Hakim, T. A., Rezk, N., Farouk, W. M., Hassan, Y. Y., Gouda, S. M. & El-Shibiny, A. (2022). Green Synthesis of Silver Nanoparticles Using *Ocimum basilicum* L. and *Hibiscus sabdariffa* L. Extracts and Their Antibacterial Activity in Combination with Phage ZCSE6 and Sensing Properties. *Journal of Inorganic and Organometallic Polymers and Materials*, 32(6), 1951–1965. <https://doi.org/10.1007/s10904-022-02234-y>
- Adhikari, A., Lamichhane, L., Adhikari, A., Gyawali, G., Acharya, D., Baral, E. R. & Chhetri, K. (2022). Green Synthesis of Silver Nanoparticles Using *Artemisia vulgaris* Extract and Its Application toward Catalytic and Metal-Sensing Activity. *Inorganics*, 10(8). <https://doi.org/10.3390/inorganics10080113>
- Ads, E. N., Rajendrasozhan, S., Hassan, S. I., Sharawy, S. M. S. & Humaidi, J. R. (2018). Phytochemical screening of different organic crude extracts from the stem bark of *Ziziphus spina-christi* (L.). *Biomedical Research (India)*, 29(8), 1645–1652. <https://doi.org/10.4066/biomedicalresearch.29-17-1668>
- Aisida, S. O., Ugwu, K., Akpa, P. A., Nwanya, A. C., Ejikeme, P. M., Botha, S., Ahmad, I., Maaza, M. & Ezema, F. I. (2019). Biogenic synthesis and antibacterial activity of controlled silver nanoparticles using an extract of *Gongronema latifolium*. *Materials Chemistry and Physics*, 237, 121859. <https://doi.org/https://doi.org/10.1016/j.matchemphys.2019.121859>
- Alduraim, N. S., Bhat, R. S., Al-Zahrani, S. A., Elnagar, D. M., Alobaid, H. M. & Daghestani, M. H. (2023). Anticancer and Antimicrobial Activity of Silver Nanoparticles Synthesized from Pods of *Acacia nilotica*. *Processes*, 11(2). <https://doi.org/10.3390/pr11020301>
- Al-Maaqar, S.M., Al-Johny, B. O., Al-Sharif, F. D., Alshareef, M., Al Kenani, N & Hussain, M. B. (2022). Sensitivity of multidrug-resistant pathogenic bacteria to ethanolic extract of *Ziziphus spina-christi* L. (Sidr) leaves. *Bioscience Research*, 19(3): 1467-1475.
- Alotibi, F. O., Ashour, E. H. & Al-Basher, G. (2020). Evaluation of the antifungal activity of *Rumex vesicarius* L. and *Ziziphus spina-christi* (L) Desf. Aqueous extracts and assessment of the morphological changes induced to certain mycophytopathogens. *Saudi Journal of Biological Sciences*, 27(10), 2818–2828. <https://doi.org/10.1016/j.sjbs.2020.06.051>
- Alsubki, R., Tabassum, H., Abudawood, M., Rabaan, A. A., Alsobaie, S. F. & Ansar, S. (2021). Green synthesis, characterization, enhanced functionality and biological evaluation of silver nanoparticles based on Coriander sativum. *Saudi Journal of Biological Sciences*, 28(4), 2102–2108. <https://doi.org/10.1016/j.sjbs.2020.12.055>
- Amin, A. R., Kassab, R. B., Abdel Moneim, A. E. & Amin, H. K. (2020). Comparison Among Garlic, Berberine, Resveratrol, Hibiscus sabdariffa, Genus *Zizyphus*, *Hesperidin*, Red Beetroot, *Catha edulis*, *Portulaca oleracea*, and Mulberry Leaves in the Treatment of Hypertension and Type 2 DM: A Comprehensive Review. *Natural Product Communications*, 15(4). <https://doi.org/10.1177/1934578X20921623>
- Anju, T. R., Parvathy, S., Valiya Veetil, M., Rosemary, J., Ansalna, T. H., Shahzabanu, M. M. & Devika, S. (2021). Green synthesis of silver nanoparticles from Aloe vera leaf extract and its antimicrobial activity. *Materials Today: Proceedings*, 43, 3956–3960. <https://doi.org/https://doi.org/10.1016/j.matpr.2021.02.665>
- Ashraf, A., Zafar, S., Zahid, K., Salahuddin Shah, M., Al-Ghanim, K. A., Al-Misned, F. & Mahboob, S. (2019). Synthesis, characterization, and antibacterial potential of silver nanoparticles synthesized from *Coriandrum sativum* L. *Journal of Infection and Public Health*, 12(2), 275–281. <https://doi.org/https://doi.org/10.1016/j.jiph.2018.11.002>
- Balciunaitiene, A., Viskelis, P., Viskelis, J., Streimikyte, P., Liaudanskas, M., Bartkiene, E., Zavistanaviciute, P., Zokaityte, E., Starkute, V., Ruzauskas, M. & Lele, V. (2021). Green synthesis of silver nanoparticles using extract of *Artemisia absinthium* L., *Humulus lupulus* L. and *Thymus vulgaris* L., physico-chemical characterization, antimicrobial and antioxidant activity. *Processes*, 9(8). <https://doi.org/10.3390/pr9081304>
- Chapagain, A., Acharya, D., Das, A. K., Chhetri, K., Oli, H. B. & Yadav, A. P. (2022). Alkaloid of *Rhynchosyilis retusa* as Green Inhibitor for Mild Steel Corrosion in 1 M H₂SO₄ Solution. *Electrochem*, 3(2), 211–224. <https://doi.org/10.3390/electrochem3020013>
- Dkhil, M. A., Al-Quraishy, S. & Moneim, A. E. A. (2018). *Ziziphus spina-christi* leaf extract pretreatment inhibits liver and spleen injury in a mouse model of sepsis via anti-oxidant and anti-inflammatory effects. *Inflammopharmacology*, 26(3), 779–791. <https://doi.org/10.1007/s10787-017-0439-8>
- Ekennia, A. C., Uduagwu, D. N., Nwaji, N. N., Olowu, O.

- J., Nwanji, O. L., Ejimofor, M., Sonde, C. U., Oje, O. O. & Igwe, D. O. (2022). Green synthesis of silver nanoparticles using leaf extract of *Euphorbia sanguine*: an in vitro study of its photocatalytic and melanogenesis inhibition activity. *Inorganic and Nano-Metal Chemistry*, 52(2), 195–203. <https://doi.org/10.1080/24701556.2021.1891100>
- El-Ansary, A., Warsy, A., Daghestani, M., Merghani, N. M., Al-Dbass, A., Bukhari, W., Al-Ojayan, B., Ibrahim, E. M., Al-Qahtani, A. M. & Bhat, R. S. (2018). Characterization, antibacterial, and neurotoxic effect of Green synthesized nanosilver using *Ziziphus spina Christi* aqueous leaf extract collected from Riyadh, Saudi Arabia. *Materials Research Express*, 5(2). <https://doi.org/10.1088/2053-1591/aaaf5f>
- El Maaiden, E., El Kharrassi, Y., Moustaid, K., Essamadi, A. K. & Nasser, B. (2019). Comparative study of phytochemical profile between *Ziziphus spina christi* and *Ziziphus lotus* from Morocco. *Journal of Food Measurement and Characterization*, 13(1), 121–130. <https://doi.org/10.1007/s11694-018-9925-y>
- ERENLER, R., GEÇER, E. N., GENÇ, N. & YANAR, D. (2021). Antioxidant activity of silver nanoparticles synthesized from *Tagetes erecta* L. leaves. *International Journal of Chemistry and Technology*, 5(2), 141–146. <https://doi.org/10.32571/ijct.1005275>
- Fouda, A., Eid, A. M., Guibal, E., Hamza, M. F., Hassan, S. E. D., Alkhalifah, D. H. M. & El-Hossary, D. (2022). Green Synthesis of Gold Nanoparticles by Aqueous Extract of *Zingiber officinale*: Characterization and Insight into Antimicrobial, Antioxidant, and In Vitro Cytotoxic Activities. *Applied Sciences (Switzerland)*, 12(24). <https://doi.org/10.3390/app122412879>
- Ghatage, M. M., Mane, P. A., Gambhir, R. P., Parkhe, V. S., Kamble, P. A., Lokhande, C. D. & Tiwari, A. P. (2023). Green synthesis of silver nanoparticles via *Aloe barbadensis miller* leaves: Anticancer, antioxidative, antimicrobial and photocatalytic properties. *Applied Surface Science Advances*, 16(October 2022), 100426. <https://doi.org/10.1016/j.apsadv.2023.100426>
- Giri, A. K., Jena, B., Biswal, B., Pradhan, A. K., Arakha, M., Acharya, S. & Acharya, L. (2022). Green synthesis and characterization of silver nanoparticles using *Eugenia roxburghii* DC. extract and activity against biofilm-producing bacteria. *Scientific Reports*, 12(1), 1–9. <https://doi.org/10.1038/s41598-022-12484-y>
- Gul, A., Baig, M. N., Ahmed, D., Najam, Z., Aslam, T. & Ali, S. (2024). Green Synthesis of Silver Nanoparticles from *Spirulina platensis* Extract: Antibacterial and Antioxidant Potential. *BioNanoScience*, 1–10. <https://doi.org/https://doi.org/10.1007/s12668-024-01473-2>
- Hembram, K. C., Kumar, R., Kandha, L., Parhi, P. K., Kundu, C. N. & Bindhani, B. K. (2018). Therapeutic prospective of plant-induced silver nanoparticles: application as antimicrobial and anticancer agent. *Artificial Cells, Nanomedicine and Biotechnology*, 46(sup3), S38–S51. <https://doi.org/10.1080/21691401.2018.1489262>
- Jomova, K., Alomar, S. Y., Alwasel, S. H., Nepovimova, E., Kuca, K. & Valko, M. (2024). Several lines of antioxidant defense against oxidative stress: antioxidant enzymes, nanomaterials with multiple enzyme-mimicking activities, and low-molecular-weight antioxidants. In *Archives of Toxicology* (Vol. 98, Issue 5). Springer Berlin Heidelberg. <https://doi.org/10.1007/s00204-024-03696-4>
- Karan, T., Gonulalan, Z., Erenler, R., Kolemen, U. & Eminagaoglu, O. (2024). Green synthesis of silver nanoparticles using *Sambucus ebulus* leaves extract: Characterization, quantitative analysis of bioactive molecules, antioxidant and antibacterial activities. *JOURNAL OF MOLECULAR STRUCTURE*, 1296. <https://doi.org/10.1016/j.molstruc.2023.136836>
- Kendel, A. & Zimmermann, B. (2020). Chemical Analysis of Pollen by FT-Raman and FTIR Spectroscopies. *Frontiers in Plant Science*, 11(March), 1–19. <https://doi.org/10.3389/fpls.2020.00352>
- Kumar, V., Singh, D. K., Mohan, S. & Hasan, S. H. (2016). Photo-induced biosynthesis of silver nanoparticles using aqueous extract of *Erigeron bonariensis* and its catalytic activity against Acridine Orange. *Journal of Photochemistry and Photobiology B: Biology*, 155, 39–50. <https://doi.org/https://doi.org/10.1016/j.jphotobiol.2015.12.011>
- Loka, C. & Lee, K. S. (2022). Enhanced Visible-Light-Driven Photocatalysis of Ag/Ag₂O/ZnO Nanocomposite Heterostructures. *Nanomaterials*, 12(15). <https://doi.org/10.3390/nano12152528>
- Luan, L. Q. & Xo, D. H. (2018). In vitro and in vivo fungicidal effects of γ -irradiation synthesized silver nanoparticles against *Phytophthora capsici* causing the foot rot disease on pepper plant. *Journal of Plant Pathology*, 100(2), 241–248. <https://doi.org/https://doi.org/10.1007/s42161-018-0064-4>
- Maduraimuthu, V., Ranishree, J. K., Gopalakrishnan, R. M., Ayyadurai, B., Raja, R. & Heese, K. (2023). Antioxidant Activities of Photoinduced Phycogenic Silver Nanoparticles and Their Potential Applications. *Antioxidants*, 12(6). <https://doi.org/10.3390/antiox12061298>
- Manikandan, D. B., Sridhar, A., Krishnasamy Sekar, R., Perumalsamy, B., Veeran, S., Arumugam, M., Karuppaiah, P. & Ramasamy, T. (2021). Green fabrication, characterization of silver nanoparticles using aqueous leaf extract of *Ocimum americanum* (Hoary Basil) and investigation of its in vitro antibacterial, antioxidant, anticancer and photocatalytic reduction. *Journal of Environmental*

- Chemical Engineering*, 9(1), 104845. <https://doi.org/https://doi.org/10.1016/j.jece.2020.104845>
- Miranda, A., Akpobolokemi, T., Chung, E., Ren, G. & Raimi-Abraham, B. T. (2022). pH Alteration in Plant-Mediated Green Synthesis and Its Resultant Impact on Antimicrobial Properties of Silver Nanoparticles (AgNPs). *Antibiotics*, 11(11). <https://doi.org/10.3390/antibiotics11111592>
- Naseem, K., Aziz, A., Khan, M. E., Ali, S. & Khalid, A. (2024). Bioinorganic metal nanoparticles and their potential applications as antimicrobial, antioxidant and catalytic agents: a review. *Reviews in Inorganic Chemistry*, 0. <https://doi.org/10.1515/revic-2023-0040>
- Noppradit, B., Chaiyosburana, S., Khupsathianwong, N., Tapachai, W. A., Wattanakanjana, Y. & Phengdaam, A. (2023). Green synthesis of silver nanoparticles using *Saccharum officinarum* leaf extract for antiviral paint. *Green Processing and Synthesis*, 12(1). <https://doi.org/10.1515/gps-2023-0172>
- Sidhu, A. K., Verma, N. & Kaushal, P. (2022). Role of Biogenic Capping Agents in the Synthesis of Metallic Nanoparticles and Evaluation of Their Therapeutic Potential. 3(January), 1–17. <https://doi.org/10.3389/fnano.2021.801620>
- Singh, C., Anand, S. K., Upadhyay, R., Pandey, N., Kumar, P., Singh, D., Tiwari, P., Saini, R., Tiwari, K. N., Mishra, S. K. & Tilak, R. (2023). Green synthesis of silver nanoparticles by root extract of *Premna integrifolia* L. and evaluation of its cytotoxic and antibacterial activity. *Materials Chemistry and Physics*, 297, 127413. <https://doi.org/https://doi.org/10.1016/j.matchemphys.2023.127413>
- Sivalingam, A. M., Pandian, A. & Rengarajan, S. (2024). Green Synthesis of Silver Nanoparticles Using *Vernonia Amygdalina* Leaf Extract: Characterization, Antioxidant, and Antibacterial Properties. *Journal of Inorganic and Organometallic Polymers and Materials*, 1–17.
- Sreelekha, E., George, B., Shyam, A., Sajina, N. & Mathew, B. (2021). A Comparative Study on the Synthesis, Characterization, and Antioxidant Activity of Green and Chemically Synthesized Silver Nanoparticles. *BioNanoScience*, 11(2), 489–496. <https://doi.org/10.1007/s12668-021-00824-7>
- Sysak, S., Czarczynska-Goslinska, B., Szyk, P., Koczorowski, T., Mlynarczyk, D. T., Szczolko, W., Lesyk, R. & Goslinski, T. (2023). Metal nanoparticle-flavonoid connections: synthesis, physicochemical and biological properties, as well as potential applications in medicine. *Nanomaterials*, 13(9), 1531.
- Tang, Q., Xia, H., Liang, W., Huo, X. & Wei, X. (2020). Synthesis and characterization of zinc oxide nanoparticles from *Morus nigra* and its anticancer activity of AGS gastric cancer cells. *Journal of Photochemistry and Photobiology B: Biology*, 202, 111698. <https://doi.org/https://doi.org/10.1016/j.jphotobiol.2019.111698>
- Wijesinghe, U., Thiripuranathar, G., Iqbal, H. & Mena, F. (2021). Biomimetic synthesis, characterization, and evaluation of fluorescence resonance energy transfer, photoluminescence, and photocatalytic activity of zinc oxide nanoparticles. *Sustainability (Switzerland)*, 13(4), 1–22. <https://doi.org/10.3390/su13042004>
- Yassin, M. A., El-Samawaty, A. E.-R. M. A., Dawoud, T. M., Abd-Elkader, O. H., Al Maary, K. S., Hatamleh, A. A. & Elgorban, A. M. (2017). Characterization and anti-*Aspergillus flavus* impact of nanoparticles synthesized by *Penicillium citrinum*. *Saudi Journal of Biological Sciences*, 24(6), 1243–1248. <https://doi.org/10.1016/j.sjbs.2016.10.004>
- Yassin, M. A., Elgorban, A. M., El-Samawaty, A. E. R. M. A. & Almunqedhi, B. M. A. (2021). Biosynthesis of silver nanoparticles using *Penicillium verrucosum* and analysis of their antifungal activity. *Saudi Journal of Biological Sciences*, 28(4), 2123–2127. <https://doi.org/10.1016/j.sjbs.2021.01.063>
- Yu, C., Tang, J., Liu, X., Ren, X., Zhen, M. & Wang, L. (2019). Green biosynthesis of silver nanoparticles using *eriobotrya japonica* (thunb.) leaf extract for reductive catalysis. *Materials*, 12(1). <https://doi.org/10.3390/ma12010189>
- Zhang, X. F., Liu, Z. G., Shen, W. & Gurunathan, S. (2016). Silver nanoparticles: Synthesis, characterization, properties, applications, and therapeutic approaches. *International Journal of Molecular Sciences*, 17(9). <https://doi.org/10.3390/ijms17091534>
- Zheljazkov, V. D., Kacaniova, M., Dincheva, I., Radoukova, T., Semerdjieva, I. B., Astatkie, T. & Schlegel, V. (2018). Essential oil composition, antioxidant and antimicrobial activity of the galbuli of six juniper species. *Industrial Crops and Products*, 124, 449–458. <https://doi.org/10.1016/j.indcrop.2018.08.013>
- Zidane, Y., Laouini, S. E., Bouafia, A., Meneceur, S., Tedjani, M. L., Alshareef, S. A., Almukhlifi, H. A., Al-Essa, K., Al-Essa, E. M., Rahman, M. M., Madkhali, O. & Mena, F. (2022). Green synthesis of multifunctional MgO@AgO/Ag₂O nanocomposite for photocatalytic degradation of methylene blue and toluidine blue. *Frontiers in Chemistry*, 10(December), 1–14. <https://doi.org/10.3389/fchem.2022.1083596>